

Article

Preparation and Characterization of Zinc Oxide Nanoparticles Using Leaf Extract of *Sambucus ebulus*

Sanaz Alamdari ^{1,*}, Morteza Sasani Ghamsari ², Chan Lee ³, Wooje Han ³,
Hyung-Ho Park ^{3,*}, Majid Jafar Tafreshi ⁴, Hosein Afarideh ⁵ and
Mohammad Hosein Majles Ara ⁶

¹ Faculty of Physics, Semnan University, P.O. Box 35195-363, Semnan, Iran

² Photonics & Quantum Technologies Research School, Nuclear Science, and Technology Research Institute, Tehran 11155-3486, Iran; msghamsari@yahoo.com

³ Department of Materials Science and Engineering, Yonsei University, 50 Yonsei-ro, Seodaemun-gu, Seoul 03722, Korea; chanlee@yonsei.ac.kr (C.L.); wooje_han@yonsei.ac.kr (W.H.)

⁴ Department of Physics, Semnan University, P.O. Box 35195-363, Semnan, Iran; m.tafreshi@semnan.ac.ir

⁵ Department of Energy Engineering and Physics, Amirkabir University of Technology, Tehran 15875-4413, Iran; hafarideh@aut.ac.ir

⁶ Applied Science Research Center(ASRC), Kharazmi University, Tehran 31979-37551, Iran; majlesara@gmail.com

* Correspondence: s.alamdari@semnan.ac.ir or alamdarianaz@gmail.com (S.A.);
hhpark@yonsei.ac.kr (H.-H.P); Tel.: +98-31533221 (S.A.); +82-21232853 (H.-H.P);
Fax: +98-23-33654081 (S.A.); +82-2-3125375 (H.-H.P)

Received: 26 March 2020; Accepted: 19 May 2020; Published: 23 May 2020



Abstract: Plants are one of the best sources to obtain a variety of natural surfactants in the field of green synthesizing material. *Sambucus ebulus*, which has unique natural properties, has been considered a promising material in traditional Asian medicine. In this context, zinc oxide nanoparticles (ZnO NPs) were prepared using *S. ebulus* leaf extract, and their physicochemical properties were investigated. X-ray diffraction (XRD) results revealed that the prepared ZnO NPs are highly crystalline, having a wurtzite crystal structure. The average crystallite size of prepared NPs was around 17 nm. Green synthesized NPs showed excellent absorption in the UV region as well as strong yellow-orange emission at room temperature. Prepared nanoparticles exhibited good antibacterial activity against various organisms and a passable photocatalytic degradation of methylene blue dye pollutants. The obtained results demonstrated that the biosynthesized ZnO NPs reveal interesting characteristics for various potential applications in the future.

Keywords: ZnO nanoparticles; *Sambucus ebulus*; extract; photocatalytic; antibacterial activity

1. Introduction

Zinc oxide (ZnO) is a well-engineered compound that has received remarkable interest globally due to its distinctive properties and usages in various applications, such as pharmaceuticals, cosmetics, photonics, and photocatalysis [1–6].

ZnO nanoparticles (NPs) can be synthesized through many physiochemical routes, such as sol-gel processes, co-precipitation, laser vaporization, microemulsion, and ball milling [7–10]

Commonly, these preparation methods face several limitations, such as the high cost of equipment, the large area required for equipment set up, and additional use of capping agents, stabilizers and toxic chemicals [11]. Most of these chemical methods are not environmentally friendly due to the use of harsh chemicals for stabilizing processes, which will bind to the ZnO NPs, and limit their biological applications [1,11]. To overcome these limitations, green chemistry procedures have attracted

significant scientific attention and have provided a new path for material researchers, because they are safe and environmentally friendly methods, which do not produce toxic by-products. Developing simple and green methods for synthesizing ZnO NPs is thus important, and remains a challenge for researchers [11,12].

According to the literature, plants extracts have been proposed as novel alternatives to chemical methods for synthesis of NPs [12–17]; for example, Iran and most parts of Asia have a rich source of valuable plants for this purpose [12,13]. It should be noted that most nanoparticles and plant extracts pose a threat to the ecosystem and human beings. Unregulated use in terms of their toxicity may affect the biological system in unanticipated ways. Better control of the synthetic parameters will undoubtedly help to improve not only the physiochemical properties of ZnO NPs but also their compatibility [14,18].

Extracts of citrus fruits or peels have been successfully used in producing metal and various metal oxide NPs, such as gold (Au) NPs, silver (Ag) NPs, and titanium dioxide (TiO₂) NPs [19–21]. In addition, several types of fruit and plant extracts have been used for the synthesis of ZnO NPs, such as *Limonia acidissima*, *Tabernaemontana divaricata*, *Cochlospermum religiosum*, *Conyza canadensis*, *Citrus maxima*, *Boswellia ovalifoliolata*, *Echinacea* spp., *Salvadora oleoides*, and *Aristolochia indica* [22–33]. Zare et al. [33] reported the influence of *Cuminum cyminum* leaf extract on ZnO NP synthesis, which showed a good crystallite structure and high sensitivity to Gram-negative bacteria. In a similar study, *Hibiscus sabdariffa* and *Acalypha indica* extracts presented suitable optical and antibacterial properties [34]. Furthermore, ZnO NPs have shown promising properties in photocatalytic applications; it has been reported that *Parkia roxburghii* extract/ZnO NPs showed excellent degradation of methylene blue (MB) and Rhodamine B dyes, reaching about 98% [34].

Sambucus ebulus (elderberry or danewort), which is a natural plant with novel nutritional properties, grows in most parts of South America, Asia, North Africa, and the United States [35]. This plant is rich in biomolecules for reducing metal ions and stabilizing nanoparticles; *S. ebulus* leaf extract contains enormous numbers of carbonyl, carboxyl, and hydroxyl groups in polyphenols and flavonoids [35]. These compounds can have a positive effect on human health because they can act as antioxidants and anti-inflammatory and anticancer agents. Due to its easy collection, natural origin, and remarkable biological properties, it could be an ideal replacement for expensive modern chemical surfactants. As mentioned, *S. ebulus* contains high amounts of natural antioxidants, such as flavonoids, lectins, anthocyanins, vitamin C, and phenolic compounds which may be considered as suitable stabilizing agents [35]. In our previous works, various ZnO nanostructures with novel properties were prepared using a chemical method; in our previous methods, we used triethanolamine (TEA) as a chemical surfactant for synthesis [36–44]. It is well-known that TEA, which is similar to many kinds of chemical surfactants, has a toxic hazard rating. In this study, we tried to use a plant extract as a natural surfactant instead of TEA. Notably, no previous study has been reported in the literature on the preparation of ZnO NPs using *S. ebulus* extract. The aim of this article is to report a novel room-temperature green synthesis of ZnO NPs using *S. ebulus* extract as a potential candidate for various applications with interesting structural, optical, photocatalytic, and antibacterial properties.

2. Materials and Methods

2.1. Materials Preparation

Young leaves of *S. ebulus* were picked in May 2018 in Sari, Mazandaran, Iran. All the chemical materials used in the experiments were purchased from Merck: zinc acetate dihydrate (99.7%) and ethanol (99.5%) as a solvent. The standard strains used for the tests were obtained from Alborz hospital at Karaj city and the University of Tarbiat Modares, Iran. Around 60 g of dried crushed leaves were added to 50 mL ethanol and left for 24 h, after which the mixture was heated and stirred at 45 °C for 2 h, and the plant extract was then filtered with Whatman No. 1 filter paper twice. The filtrate was collected and kept at 4 °C. This prepared extract was directly used in the synthesis experiments. 1 M

zinc acetate dihydrate was dissolved in 20 mL absolute ethanol and kept under continuous stirring for 30 min [37–44]. Approximately 2 mL of extract (as a natural surfactant) was added to the solution, followed by stirring for 2 h at 80 °C; the suspension was centrifuged at 7168 g for 15 min, and the precipitate was dried at 60 °C in a hot air oven until dried NPs were obtained. The prepared NPs were calcined at 450 °C for 2 h. A schematic representation of the experimental work and possible chemical bond formed between the extracted molecules and zinc oxide are shown in Figure 1.

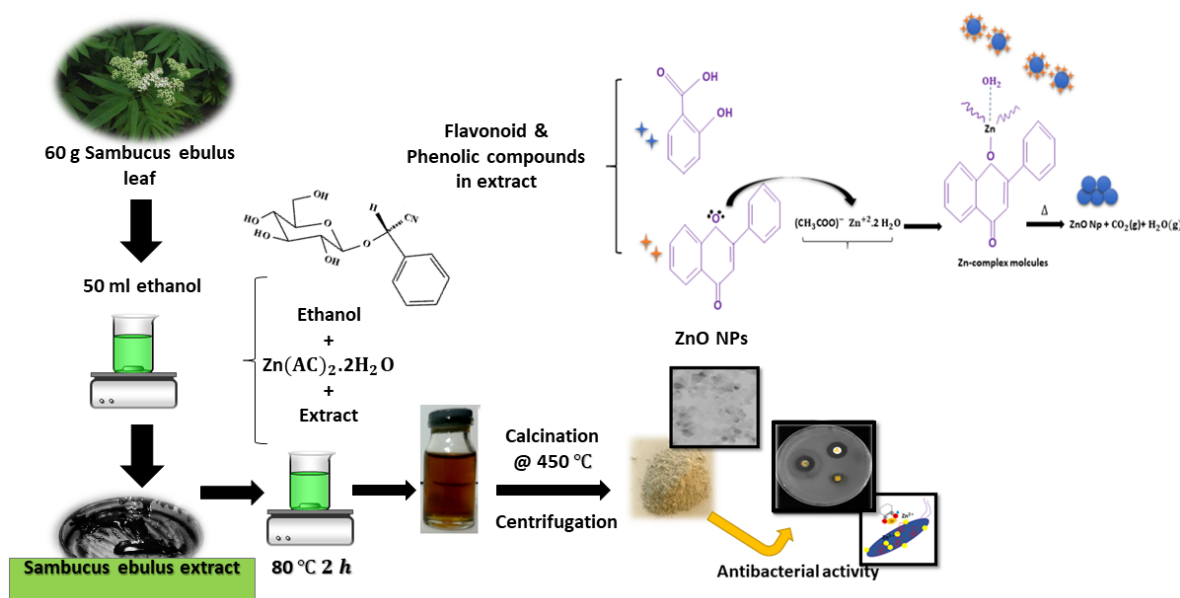


Figure 1. A schematic illustration of the synthetic route for production of ZnO nanoparticles (NPs).

2.2. Antibacterial Activity Test

The antibacterial activity of the biosynthesized ZnO NPs against pathogenic microorganisms, namely Gram-positive *Bacillus cereus* (KNIH28) and *Staphylococcus aureus* (ATCC6538 P), and Gram-negative *Escherichia coli* (*E. coli*) ATCC27853, was carried out on Muller–Hilton agar dishes using the disk diffusion method [45]. Nutrient agar broth (Himedia, Bombay) was used as bacterial culture medium in the bacterial assays. Pure cultures of the microorganisms were provided by the Alborz hospital, Karaj, Iran. The bacterial pathogens were freshly incubated for 4 h to standardize the culture to McFarland standards (10^6 CFU/mL).

All of the chemicals used for the cell culturing were of analytical grade. Cells were grown in agar media and humidified incubator at 37 °C under 5% CO₂. The concentration of bacterial cells was adjusted to 10^6 CFU/mL, and ciprofloxacin (10 µg/disc) was used as a standard. Paper disks (6 mm diameter, Whatman No. 1 filter paper) infused with 100 µg/mL concentrations of prepared ZnO NPs and pure extract (10 µg/mL) suspended in deionized water were used to ascertain the antibacterial activity, followed by incubation at 37 °C for a period of 24 h. Inhibition zones, that formed around the disk, were investigated by measuring the corresponding diameter. The antibacterial experiments were repeated three times.

2.3. Antioxidant Activity

The antioxidant activity was determined using the hydrogen peroxide (H₂O₂) free radical scavenging assay [46]. A quantity of 1 mL (with various concentrations) of the biosynthesized ZnO NPs and ascorbic acid as a standard were mixed with 50 mM (0.6 mL) H₂O₂ solution and then incubated at room temperature for 5 min. Absorbance was detected with a UV-vis spectrophotometer at 230 nm.

Phosphate-buffered saline without H₂O₂ was used as a blank test [46]. The inhibition percentage of hydrogen peroxide scavenging was obtained using the following equation:

$$\% \text{H}_2\text{O}_2 \text{ free radicals} = \left\{ 1 - \left(\frac{A_s}{A_c} \right) \right\} \times 100 \quad (1)$$

where A_c is the absorbance of the control and A_s is the absorbance of the sample.

2.4. Photocatalytic Activity

The photocatalytic activity of the biosynthesized ZnO NPs was investigated via the photocatalytic degradation of MB (a dye normally resistant to biodegradation). The photocatalytic experiments were performed under UV light (24 W UV lamp, 360 nm) irradiation. The photocatalytic decomposition of MB solution (50 ppm) by ZnO NPs as a photocatalyst (0.02 g) was performed in a 100 mL beaker at 35 °C under UV irradiation and continuous stirring to achieve the homogeneity of the solution. Absorbance was measured with a UV-Vis spectrophotometer.

2.5. Analytical Methods

The X-ray diffraction (XRD) pattern of ZnO NPs was recorded using a PANalytical PW3050/60 X-ray diffractometer equipped with Cu-K α radiation source ($\lambda = 1.5406 \text{ \AA}$) operated at 40 kV and 30 mA. Transmission electron microscopy (TEM; Philips CM120), field emission scanning electron microscopy (FE-SEM; Mira3 Tescan), energy-dispersive X-ray spectroscopy (EDX; Mira3 Tescan), and X-ray photoelectron spectroscopy (XPS; Thermo Scientific K-Alpha) were employed to investigate the morphology and topography of the samples along with elemental chemical surface analysis.

The FE-SEM instrument was operated at an accelerating voltage at 10 kV. The synthesized NPs were subjected to UV, Fourier-transform infrared (FTIR; range 4000–400 cm⁻¹), and photoluminescence (PL; range 200–800 nm) spectroscopy (UV-visible spectrophotometer, PerkinElmer and Cary fluorescence spectrophotometer) to survey the optical properties, functional groups, and structural defects. An electron paramagnetic resonance (EPR) investigation on a Bruker ELEXSYS E500 X-band (~9.45 GHz) spectrometer was conducted to study the paramagnetic defects in the structure. The GC-MS analysis of the plant extract was conducted using an Agilent 7890 A instrument under computer control at 70 eV that comprises an AOC-20i auto-sampler and a gas chromatograph interfaced to a mass spectrometer (GC-MS) equipped with an Agilent 5975 C fused capillary column (30 \times 0.25 μm ID \times 0.25 μm df). For GC-MS detection, an electron ionization system was operated in electron impact mode with an ionization energy of 70 eV. Helium gas (99.999%) was used as a carrier gas at a constant flow rate of 1 mL/min, and an injection volume of 2 μL was employed (a split ratio of 10:1). The injector temperature was maintained at 260 °C. The ion-source temperature was kept at 270 °C. The oven temperature was programmed from 40 °C with an increase rate of 3 °C/min to 250 °C. Surface potential was investigated using a Malvern Zetasizer Nano-series (Malvern Instruments Zen 3600, Malvern, UK)

3. Results and Discussion

3.1. Physicochemical Characterisation

The XRD pattern of the biosynthesized ZnO NPs presented in Figure 2a reveals well-defined relatively broad peaks with high intensity which indicates the formation of nanocrystalline phase. The observed peaks are indexed within the hexagonal ZnO wurtzite-type structure, in agreement with Joint Committee on Powder Diffraction Standards (JCPDS) card no. 36–1451 [38]. No additional peaks can be detected within the resolution limit of the X-ray diffractometer, thereby confirming the formation of single ZnO phase. Using the Debye–Scherrer formula ($D = 0.9 \lambda / \beta \cos \theta$, where θ is the diffraction angle, $\lambda = 1.5406 \text{ \AA}$, and β is the peak width at half maximum), crystallite size of prepared ZnO nanoparticles was calculated around 17 nm [38]; also, lattice parameters (a , c) were found to be about 3.306 and 5.199, respectively.

The elemental information of the synthesized ZnO NPs was confirmed by EDX (Figure 2b); the spectrum indicates the existence of Zn and O elements which confirms again the purity of the prepared ZnO NPs.

The analysis of EPR curve based on the calculated g-values from a spectrum formed of a symmetrical Lorentzian shape, indicated the presence of two narrow resonances: one at g-value ~1.985 and the other at g-value ~1.987, corresponding to shallow donors and singly ionized oxygen vacancies, respectively (Figure 2c) [47,48].

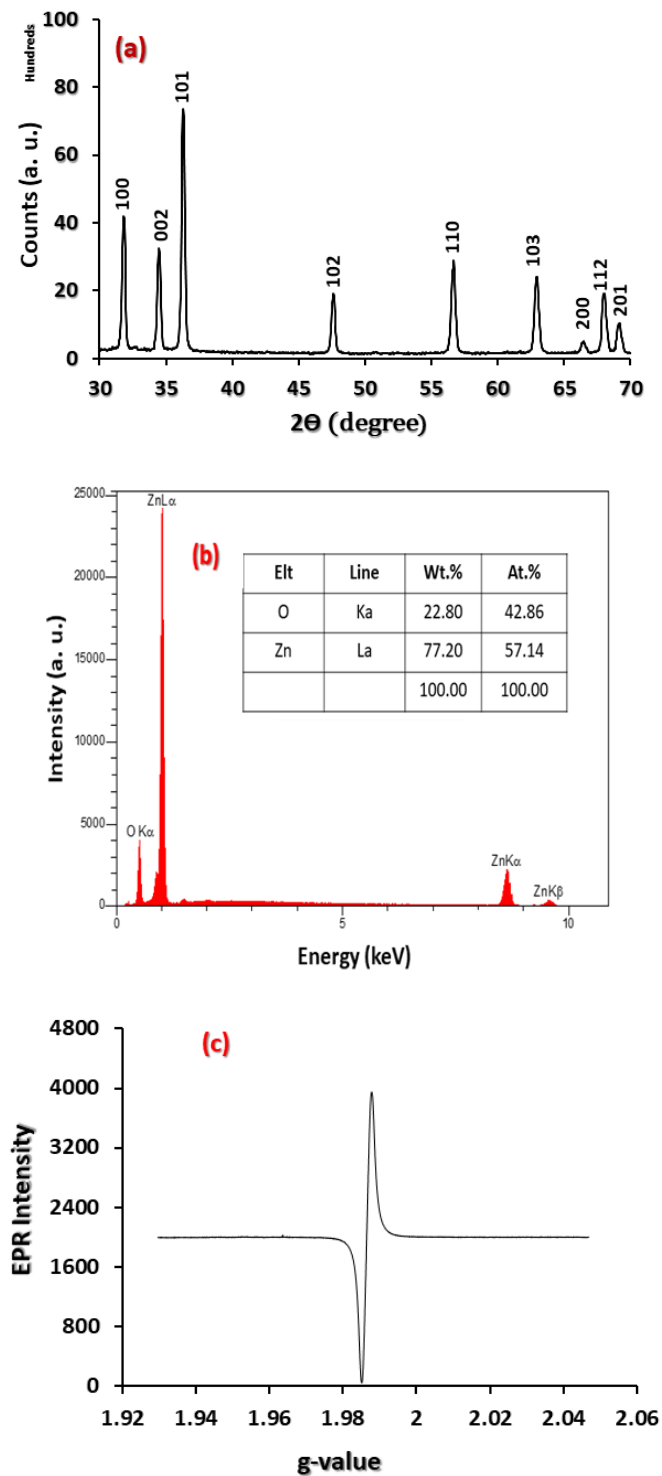


Figure 2. Cont.

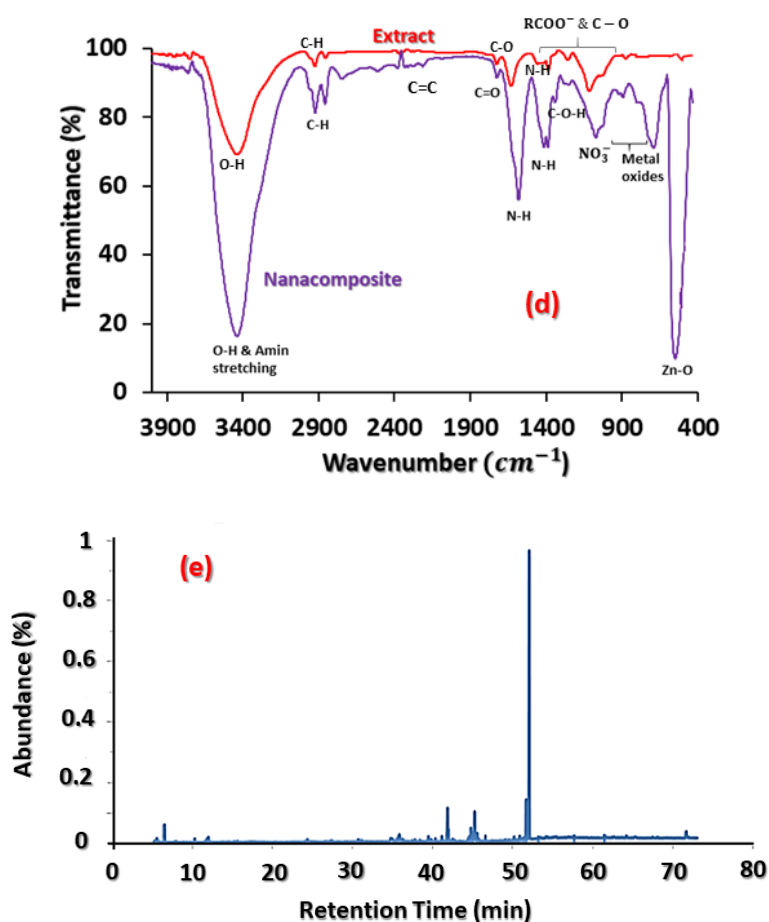


Figure 2. (a) X-ray diffraction pattern; (b) energy-dispersive X-ray spectroscopy spectrum; (c) electron paramagnetic resonance (EPR) of ZnO NPs; and (d) Fourier-transform infrared spectroscopy spectra of ZnO nanoparticles (purple line), *S. ebulus* extract (red line); and (e) typical chromatogram of the extract.

FTIR analysis helped to identify functional groups existing in the plant extract that contribute to the mechanism of bonding with ZnO NPs. As we mentioned previously, *S. ebulus* extract contains high amounts of polyphenolic derivatives, such as flavonoids, anthocyanins, and cyanidin-3-glucoside, which are considered potential bioactive compounds for therapeutic treatments and to act as reducing agents [8–15]. A comparison between the FTIR spectrum of the plant extract and that of the biosynthesized ZnO NPs is shown in Figure 2d. Accordingly, the FTIR spectrum of the plant extract exhibited several peaks at 3429, 2846, 2921, 1700, 1670, 1527, 1383, 1242, 1076, 1380, 1249, 1110, and 1024 cm^{-1} . The peaks at 3429 (O-H), 1527–1670 (N-H), and 1076 (C-O) or 880–1380 (RCOO) cm^{-1} are related to alkaloids, flavonoids, and phenolic compounds, respectively [49–52], whereas the broad stretching band at 3429 cm^{-1} indicates the presence of hydrogen-bonded groups. These results signify the existence of flavonoid derivatives in the *S. ebulus* extract. Any shift or change in the position and intensity of peaks in the sample spectrum can be correlated with the interaction of the functional groups of the flavonoids and phenols with the ZnO NPs. It can be mentioned that functional groups in the extract donate electrons that could reduce zinc ions (Zn^{2+} to Zn^{+1}) and finally zinc NPs (Zn^0). Moreover, the negative functional groups present in the extract could have a stabilizing effect. FTIR spectra of the biosynthesized ZnO NPs showed a small shift with slight changes in some related peaks and in their intensities, suggesting that the major biomolecules from the extract were capped or bonded to the surface of ZnO NPs. The major peak for the plant extract shifting from 3429 to 3426 cm^{-1} in ZnO was assigned to the O-H of the phenol groups and $-\text{NH}_2$ stretching vibrations, while another peak shifted from 1668 to 1579 cm^{-1} was ascribed to N-H binding. The appearance of new peaks at 700 and 2212–2230 cm^{-1} proved that ZnO NPs underwent C-H and C=C out-of-plane bending, respectively.

Furthermore, the FTIR spectrum of the biosynthesized ZnO NPs showed a sharp and intense band at 546 cm^{-1} , indicating the existence of Zn-O vibrations [52]. The FTIR results demonstrated that phenol and flavonoid compounds were abundant in the prepared extract and ZnO NPs. In addition, according to the GC-MS technique and Table 1, the most important compounds in the extract were carbonyl acids, ethers, and phenolic compounds.

Table 1. Compounds contained in the alcoholic extract of *S. ebulus*.

Compound	Retention Time (min)	%	Compound	Retention Time (min)	%
Acetic acid	5.50	1.20	14-methyl-Pentadecanoic acid, methyl ester	41.12	0.67
1,3-dimethoxy- Propane	5.60	0.17	n-Hexadecanoic acid	41.81	9.3
1-Butanol	6.41	2.38	Hexadecanoic acid, ethyl ester	42.43	0.33
1,1-diethoxy-2-Propanone	11.68	0.66	9Z,12Z-Octadecadienoic acid, methyl ester	44.39	0.36
Isovaleric acid	12.01	3.52	9Z,12Z,15Z-Octadecatrienoic acid, methyl ester	44.52	1.2
4-vinylphenol	24.27	1.6	Phytol	44.74	3.08
D(-)-Quinic acid	34.76	0.32	α -Linolenic acid	45.21	8.2
Pentanoic acid	36.22	0.28	Octadecanoic acid	45.52	2.62
(-)-Loliolide	41.03	0.42	9Z,12Z,15Z-Octadecatrienoic acid, ethyl ester,	44.52	0.9
Neophytadiene	39.421	1.02	Mono(2-ethylhexyl) phthalate	52.02	51.41
9-Methyl-3,4-dihydro-2H-pyrido(1,2-a)pyrimidin-2-one	39.76	2.50	Octadecanoic acid (stearic acid)	45.52	2.57
14-methyl-Pentadecanoic acid, methyl ester	41.12	0.80	D-alpha-Tocopherol(Vitamin E)	64.15	0.69
Lignocaine	41.03	0.42	22,23 -dihydro Stigmasterol	71.65	3.38

There are many advantages of applying natural plants in NP synthesis, including coating NPs with different pharmacological species (such as phenolic and polyphenolic compounds) on the metal oxide layer, which facilitates the bonding of NPs with the receptors on bacterial membranes. The *S. ebulus* extract is rich in such compounds, which are responsible for enhancing the antibacterial properties of ZnO NPs. The possible mechanism for the formation of ZnO NPs using the plant extract could be related to the flavonoid/phenolic molecules reacting with Zn^{2+} ions through the donor-acceptor mechanism. Oxygen or hydroxyl compounds present in the plant extract tend to donate an electron to electrophile Zn complexes resulting in oxidation of OH groups and reduction of electron deficient zinc ions to zinc atoms (Figure 1).

The synthesized NPs were investigated by XPS surface analysis; Figure 3 depicts a full survey scan in the range 0–1100 eV. Two intense peaks located at ~ 1024 and 1044 eV were observed, which are attributed to the Zn $2p_{3/2}$ and Zn $2p_{1/2}$, respectively, corresponding to Zn-O bonding within the hexagonal wurtzite-type structure [53,54]. The O1s peak was also present in the spectrum at ~ 529 – 530 eV, corresponding to Zn-O bonds in the intrinsic sites of the ZnO matrix, which is in good agreement with the FTIR spectrum of the biosynthesized ZnO NPs (sharp and intense band at 546 cm^{-1} , which indicates the existence of Zn-O vibrations).

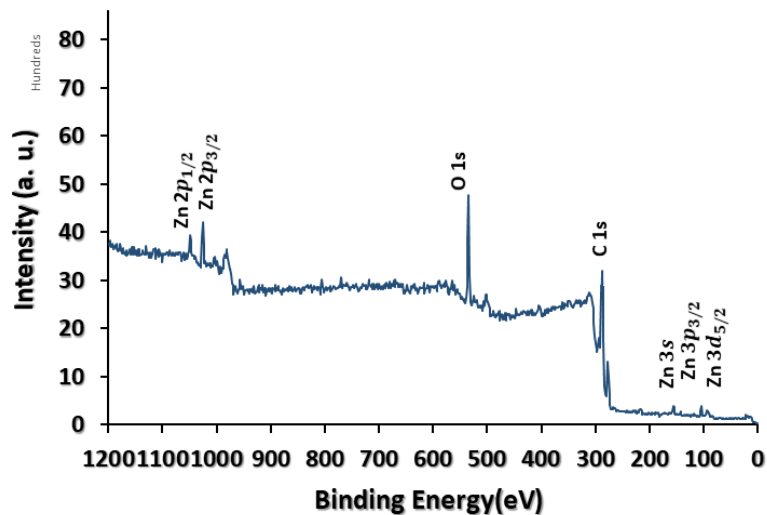


Figure 3. X-ray photoelectron spectroscopy spectrum of the biosynthesized ZnO NPs.

3.2. Optical Characterisation

Figure 4a shows the absorption spectrum of the biosynthesized ZnO NPs with an absorption peak at around 376 nm, which was assigned to the band-gap absorption of ZnO, while the very weak peak at 350 nm could be related to the presence of *S. ebulus* leaf extract. The energy band gap was found to be ~3.3 eV using the formula $E = hc/\lambda$, where λ is the wavelength, $h = 6.626 \times 10^{-34}$ Js (Planck's constant), and $c = 3 \times 10^8$ m/s, which is in good agreement with the reported values in the literature [42,44].

Moreover, using UV-vis diffuse reflectance spectroscopy (Figure 4b), the band-gap energy of the biosynthesized ZnO NPs was calculated using the Kubelka–Munk equation [55]:

$$F(R) = \frac{(1 - R)^2}{2R} \quad (2)$$

where R is the reflectance. By plotting $(F(R) \times E)^{1/2}$ as a function of energy, the value of the band gap was obtained to be ~3.3 eV (Figure 4b). The strong absorption in the UV region demonstrated that the biosynthesized ZnO NPs has a good capacity for UV-protection applications [24]. For example, the skin is one of the important protective barriers of the body and various events, such as trauma, cuts, and burns, can damage this natural layer. In these cases, a special cover must be used in the process of wound healing to repair the skin, improve the wound, protect it from UV rays, and reduce the risk of wound infection.

The PL spectrum of ZnO normally consists of two main emission peaks: (1) a UV peak near the band-edge emission and (2) a visible peak resulting from deep level emission (DLE) bands [38,56]. Some optically active intrinsic defects influence the optical properties of ZnO, and different kinds of defects are created during synthesis, growth, and/or upon annealing. The PL spectra of bare ZnO and biosynthesized ZnO using the plant extract are shown in Figure 4c,d, respectively. A broad blue emission peak centered at ~478 nm can be observed for the bare ZnO, which is normally associated with Zn defects, such as transitions from Zn_i levels (or conduction band) to valence band or V_{Zn} states (Figure 4c), while in Figure 4d, the PL spectrum of the biosynthesized ZnO using the plant extract is composed of a weak UV band at around 402 nm and an intense orange band at around 598 nm. UV emission is related to near band-edge transition, exciton-exciton collision, and free exciton recombination. The UV emission is attributed to transitions between Zn_i to the valence band [38], while yellow-orange emission is generally attributed to the DLE bands and excess oxygen, such as the transition between the vacancies and interstitials of neutral and singly ionized oxygen [38]. In n-type ZnO, acceptor-like defects (O_i) are easier to form, which enables the transition between different band-gap energies. Yellow-orange luminescent materials are widely used in optical and medical

treatments, and luminescent nanoproducts with potential bio-applications have gained great interest during the past years [57]. It can be concluded that during the chemical interaction between the plant extract molecules and ZnO NPs, some defects were passivated, which influenced the defect density and emission properties. As we mentioned previously, *S. ebulus* extract is rich in antioxidants (such as phenols and flavonols) through their carboxyl groups with binding to ZnO NPs, which can produce new levels or defects in the band gap of the host structure and, finally, influence the emission of ZnO. It is worth mentioning that many hundred years ago, *Sambucus ebulus* extract was used as a natural dye for textile applications; it is reported that silk fabrics were dyed successfully sing natural dyes extracted from *Sambucus ebulus* fruit [55].

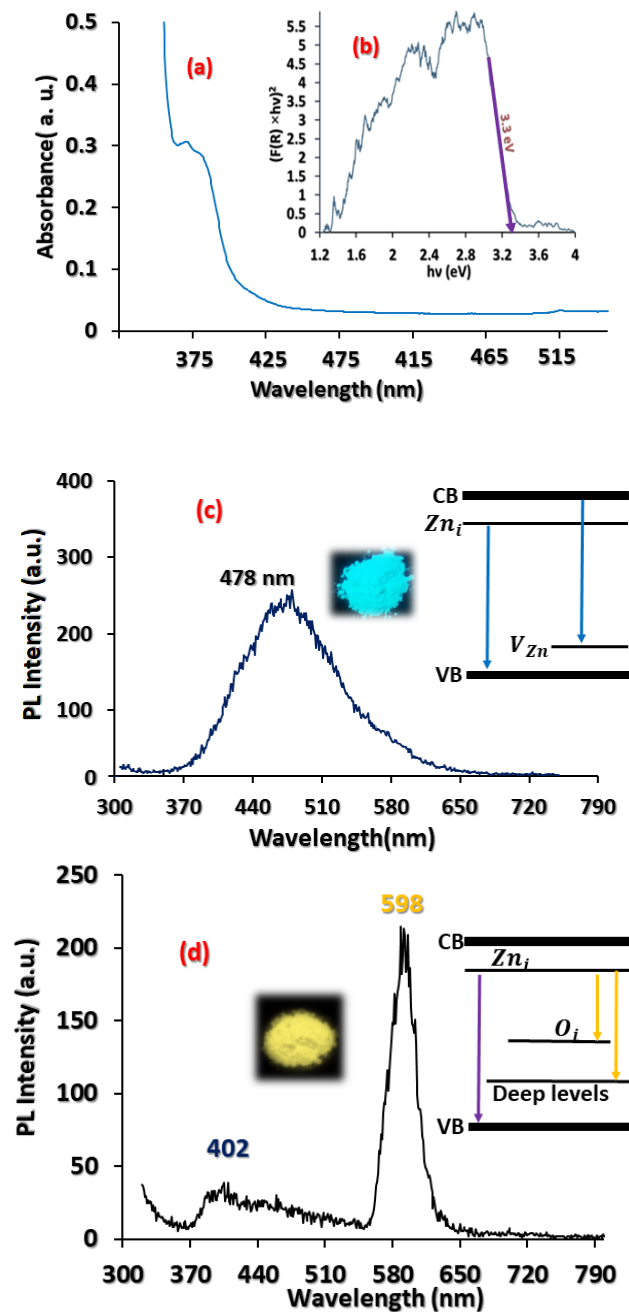


Figure 4. (a) UV absorbance and (b) optical energy band gap energy of the biosynthesized ZnO NPs using *S. ebulus* leaf extract. Photoluminescence spectra of (c) bare ZnO and (d) the ZnO nanoparticles.

3.3. Microstructural Characterisation

The uniform distribution and almost spherically shaped ZnO NPs can be observed in the FE-SEM image in Figure 5a. Some NPs are present with a hexagonal shape and the average particle size is around 40–45 nm. The NPs were dispersed in ethanol and sonicated in an ultrasonic bath for 20 min for TEM analysis. The TEM image in Figure 5b clearly shows that the NPs are mostly spherical with a size ranging from 25 to 30 nm. The selected area electron diffraction pattern, depicted in Figure 5b, confirms the crystalline nature of the biosynthesized ZnO NPs.

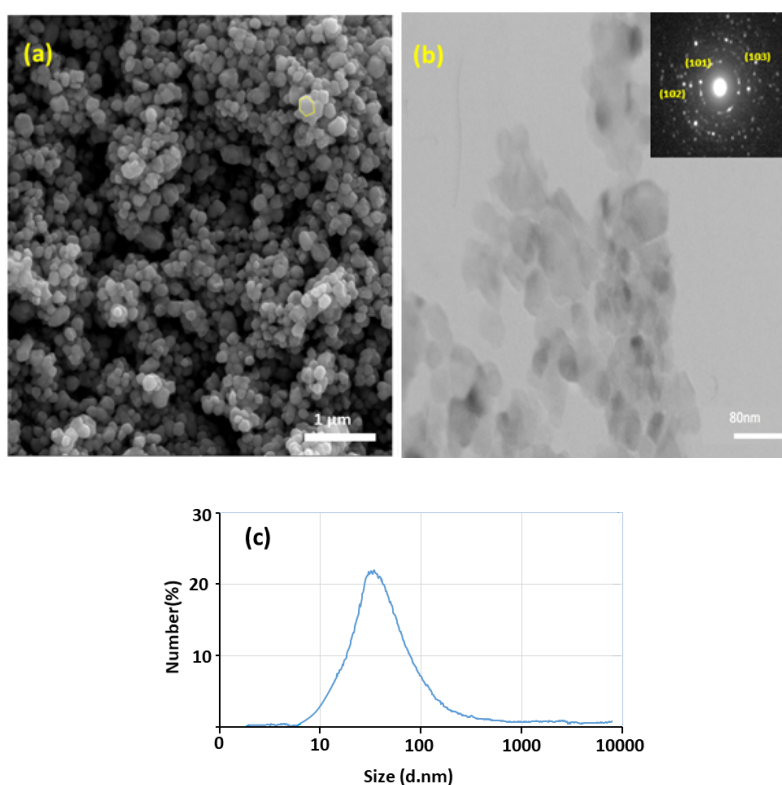


Figure 5. (a) Field emission scanning electron microscopy and (b) transmission electron microscopy images, and (c) size distribution by dynamic light scattering of the biosynthesized ZnO NPs.

According to the dynamic light scattering (DLS) technique (Figure 5c), the average size of the NPs is around 65 ± 4 nm.

It is known that the physicochemical properties of nanomaterials, including size, shape, surface area, zeta potential, and composition greatly effect on their toxicological effects. In this regard, ZnO NPs induce a significant cytotoxicity in a size-dependent trend; particularly soluble and smaller NPs provide more useful toxicological information on nanomaterials. ZnO-NP antimicrobial activity is significantly affected by particles' morphology and size, as well as concentration. The smaller the NP size, the higher their toxic effects on microorganisms, which have relatively large interfacial area and can easily penetrate bacterial membranes, thereby increasing their antibacterial effectiveness. The biosynthesized ZnO NPs used in the present work present an average diameter of 55–75 nm. It is reported that spherical shape nanoparticles (with average 21 nm size) were obtained using plant extract of *Ocimum americanum*, which showed significant antimicrobial activity against Gram-positive, Gram-negative, and fungal pathogens [24]. ZnO NPs prepared using aqueous *Tabernaemontana divaricata* green leaf extract showed a spherical shape with particle size ranging from 20 to 50 nm [25]. A higher antibacterial activity against *S. aureus* and *E. coli* and lesser antibacterial activity against *Salmonella Paratyphi* (*S. paratyphi*) compared to the standard pharmaceutical formulation, was also observed. ZnO NPs prepared using pomelo fruit juice with an average particle size of about 10–20 nm showed significant antibacterial

activity against pathogenic strains such as *S. aureus* and *K. aerogenes* and a less significant role in *E. coli* pathogenic bacterial strains [26]. ZnO NPs green synthesized from *Aristolochia indica* of size 22.5 nm exhibited remarkable bactericidal activity [27].

A zeta-potential study was carried out to detect the surface charge and stability of the prepared NPs and indicated the presence of a distinct peak at -38 mV, which suggests that the synthesized NPs have good stability. This means that the capping molecules present on the surface of biosynthesized ZnO NPs are mainly comprised of negatively charged groups and also responsible for moderate stability of the nanoparticles. The rich source of proteins and flavonoids in the extract may be responsible for the reduction of metal ions and efficient stabilization of ZnO NPs.

3.4. Photocatalytic Tests

Photocatalytic technology is an important technique for eliminating dyes in sewage water. The photocatalytic degradation characteristics of the biosynthesized NPs in MB dye solution was conducted under UV irradiation. Under irradiation, electrons through the valence band are excited and travel to the conduction band, which creates holes in the valence band. Generally, the electrons form O_2^- species through reaction with oxygen, while the holes form hydroxyl radicals through reaction with OH ions. Hence, oxidizing species can attack and oxidize organic pollutants. Usually, the proper photocatalytic activity of ZnO products can be related to the number of defects [58,59].

The degradation rate of MB was calculated as follow [60]:

$$\text{degradation \%} = (A_0 - A)/A_0 \times 100 \quad (3)$$

where A_0 is the absorbance at $t = 0$ min and A is the absorbance after treatment. According to Figure 6a, it is obvious that the absorbance peak was reduced significantly (after 200 min). Indeed, the biosynthesized ZnO NPs show a noticeable reduction in intensity, thus indicating the degradation of the dye molecules. Figure 6b depicts the degree of degradation of the MB solution obtained with ZnO NPs after UV radiation over time. It is obvious that the maximum degradation of around 80% was obtained after 200 min. In a similar study on photocatalytic degradation of MB dye with ZnO-*Camellia sinensis* NPs, the same result of approximately 80% degradation in 120 min was obtained [61].

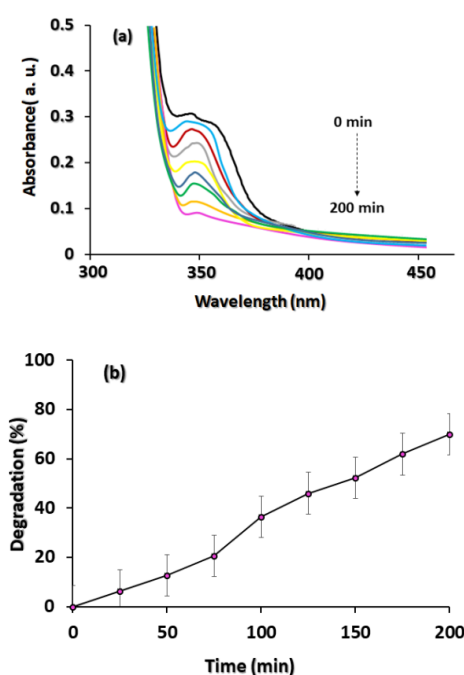


Figure 6. (a) UV absorption spectra (black line: 0 min to purple line: 200 min in 25 min increments) and (b) degradation percentage of methylene blue (50 ppm) by photocatalysis with the biosynthesized ZnO NPs under UV irradiation.

3.5. Antibacterial and Antioxidant Properties

Since no previous work has been reported yet on *S. ebulus* extract-loaded ZnO NPs, some antibacterial properties in this study were compared with similar studies but using different natural extracts and commercial/chemical synthesized ZnO [62–83]. The antibacterial activity of the biosynthesized ZnO NPs using leaf extract and the pure extract was investigated on *B. cereus*, *S. aureus*, and *E. coli* bacteria (Figure 7a). The biosynthesized ZnO NPs exhibited antibacterial activity over all three bacteria, but was higher for Gram-negative bacteria compared to Gram-positive bacteria. Moreover, the ZnO NPs exhibited a considerable zone of inhibition for *E. coli* and *B. cereus* compared with *S. aureus*. Similar observations were reported for the antibacterial properties of ZnO NPs/plant extracts against *E. coli* strains [62,63]. The results show more activity toward Gram-negative bacteria, which can be due to the existence of a thick rigid layer that surrounds their cells. This effect has already been reported [63].

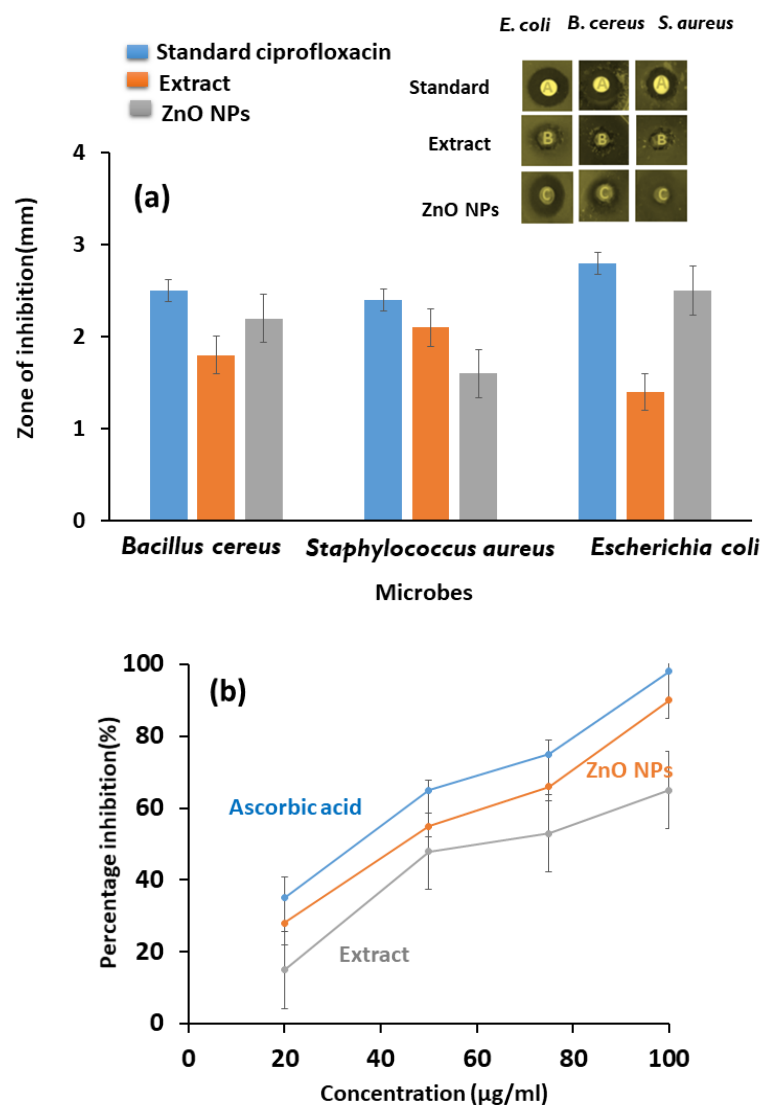


Figure 7. Cont.

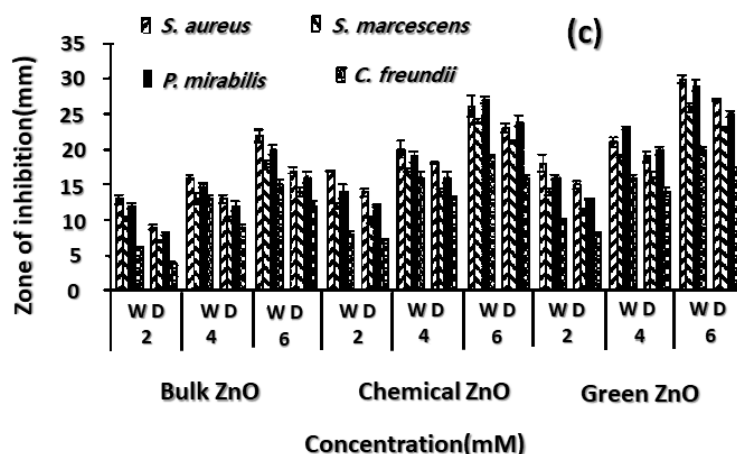


Figure 7. (a) Antibacterial activity of the biosynthesized ZnO NPs, *S. ebulus* extract, and ciprofloxacin against *B. cereus*, *S. aureus*, and *E. coli*, (b) H_2O_2 free radical scavenging activity of the biosynthesized ZnO NPs, *S. ebulus* extract, and ascorbic acid, and (c) antibacterial activity against various pathogens of green synthesized ZnO NPs when compared to chemical ZnO NPs [83].

The antioxidant properties of the biosynthesized NPs are presented in Figure 7b. The H_2O_2 activity of ascorbic acid (standard), the biosynthesized ZnO NPs, and leaf extract exhibited IC_{50} values of 36, 43, and 62 $\mu\text{g/mL}$, respectively. Enhancement in the antioxidant properties of the biosynthesized ZnO NPs in comparison with the leaf extract could be a consequence of metal or Zn ions existing in the structure. Generally, it has been reported that phenolic species existing in plant extracts have revealed high antioxidant properties, which is an important characteristic for bio-applications [76]. For comparison, strong antioxidant activity has been found in ZnO NPs isolated from extracts of *Allium sativum*, *Rosmarinus officinalis*, and *Ocimum basilicum* for comparison [77].

Microorganisms are protected by a cell membrane covering them and through this membrane sufficient nutrient are transported [64,65]. Figure 8 shows different mechanisms adopted by Gram-negative bacteria for attachment of ZnO NPs and their transport inside the bacteria cell. Gram-negative bacteria have a triple thin layer of peptidoglycan compared with Gram-positive bacteria and show less toleration to nanoparticle interaction with the cell membrane. According to Figure 8, a Gram-negative bacterium (such as *E. coli*) has a layer of peptidoglycan in its cell wall where porins are present in the outer layer. Porins are a family of proteins that exist in the outer peptidoglycan layer that helps passive diffusion of NPs inside the cell. ZnO NPs prefer to dissolve in the aqueous medium containing bacteria and release Zn^{2+} ion (because of free energy) [78]. The interaction between zinc ions and the cell wall results in a change in surface tension which leads to the membrane depolarization at the point of contact. As a result, the bacterial membrane shows abnormal textures such as membrane rupture or membrane blebs. ZnO NPs, as an antibacterial agent, act with a series of mechanisms; in this way, cell membrane integrity loss (induced by disruption of the phospholipid bilayer) and oxidative stress (induced by reactive oxygen species (ROS) generation which causes cell death by inhibiting) are two important events (Figure 8) [64,79]. ZnO and its related defects can be easily activated by UV and visible light, which leads to electron-hole pair generation [35]; the formed excitons could increase ROS concentration. ROS molecules could be superoxide, hydroxyl, singlet oxygen, and peroxide ions which are produced on the surface of NPs and possess high electronegativity that can enhance the antimicrobial activity. For example, the generated H_2O_2 molecules can penetrate into the bacterial cell membrane inducing structural changes to membranes and hence disturbing nutrient/protein transport and causing bacteria death. OH radicals are negatively charged, and thus cannot penetrate the outer cell membrane of *E. coli*, which is also negatively charged, and remain in direct contact with the outer surface of the bacterium [66–68]. The entry of ZnO NPs into the cell leads to integrity loss of phospholipid layer and blebbing of intracellular elements resulting in cell death. Nanoparticles react with membrane proteins and inactivate them decreasing membrane permeability and causing cell

death. The antibacterial activities of ZnO NPs strongly depend on shape, size, powder concentration, specific surface area, zeta potential, etc. For example, it is reported that ZnO NPs with positive surface potential showed higher antimicrobial properties compared with ZnO NPs of the same size but with negative surface potential [80]. Furthermore, it is reported that small-sized nanoparticles can penetrate the bacterial membrane easily and spherically shaped ZnO NPs release Zn^{2+} ions more effectively than rod-shaped ions [81,82].

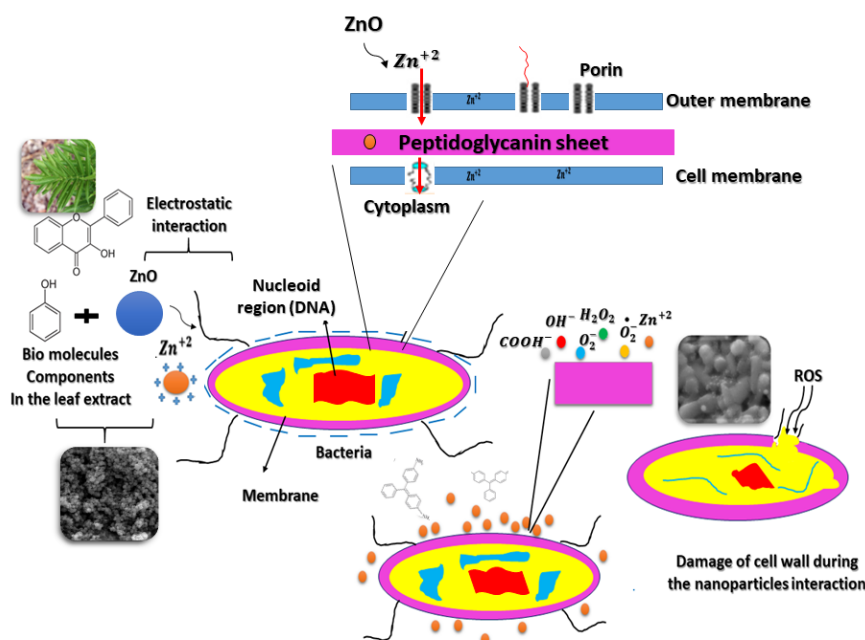


Figure 8. A schematic diagram of the antibacterial activity mechanism.

As observed above, biosynthesized ZnO NPs depict better antibacterial activity against various microorganisms when compared to pure extract.

Previous studies imply that green ZnO nanoparticles showed more enhanced biocidal activity against various pathogens when compared to chemical ZnO nanoparticles [83]; furthermore, Susheela et al. reported that green synthesized nanoparticles show more effective antimicrobial activity than those of plant extracts [84].

Surface modifying reagent molecules result in differences in the release of Zn^{2+} ions and the production of reactive oxygen species (ROS). *S. ebulus* leaf extract contains enormous numbers of carbonyl, carboxyl, and hydroxyl groups in polyphenols and flavonoids [35,69–71]. These compounds can have a positive effect on human health because they can act as antioxidants and anti-inflammatory and anticancer agents. Indeed, these compounds present a wide range of biological activities, and the presence of abundant hydroxyl and carbonyl groups is responsible for antibacterial applications [69–71]. These compounds can affect the release of Zn^{2+} and the production of ROS. The existence of these compounds in the extract and the surface helps ZnO NPs to adhere to the bacterial cell membranes. The chemical interaction between the extract molecules and ZnO NPs enhance the reactivity of NPs and improves penetration via bonding to the surface of the bacteria. Plant extract compounds attach to the surface of the bacteria and create new pathways near the surface for better transportation of or penetration by ions. For example, hydrogen in these compounds acts as both an oxidizing and a reducing agent (due to its two distinct oxidation states) which can easily form many bonds with other molecules [72,73].

In a recent study, it was found that *Albizia lebbek* stem bark increased the antibacterial effect of biosynthesized ZnO NPs [74]. In another investigation, ZnO NPs (100–190 nm) were synthesized using *Trifolium pratense* flower extract and the high zone of their growth inhibition (29–31 mm) against *E. coli*, and *S. aureus* at ~1200 $\mu\text{g}/\text{mL}$ was obtained [20]. In the work performed by Gunalan et al. [75],

the biosynthesized ZnO NPs using *Aloe vera* extract showed enhanced antibacterial properties compared with chemically prepared ZnO NPs [75]. On the other hand, Arvanag et al. [76] synthesized ZnO NPs with *Silybum marianum* L. seed extract and reported effective growth inhibition of Gram-negative *E. coli*. In another study, silver-loaded ZnO nanowires were synthesized under UV light and exhibited strong antibacterial effects against *E. coli* [73]; it was found that UV exposure caused more ROS species formation that increased antibacterial activity. In our study, we achieved lower used concentration values of *S. ebulus* leaf extract-loaded ZnO NPs that exhibited more effective antimicrobial activity against *E. coli*. It should be mentioned that despite the novel properties of *Sambucus ebulus*, similar to many kinds of plants, they may exhibit toxicity when large amounts of them are used [18]. Briefly, it can be concluded that combining ZnO NPs with *S. ebulus* extract is a simple, safe, and cost-effective approach for producing new materials with great potential for future biomedical and industrial applications.

4. Conclusions

In this study, ZnO NPs were successfully prepared through a green synthesis method using *S. ebulus* leaf extract, which showed interesting properties. X-ray diffraction analysis confirmed the formation of a ZnO hexagonal wurtzite structure with a crystallite size of 17 nm. The prepared ZnO NPs exhibited high UV absorbance, strong orange emission at room temperature, and acceptable photocatalytic degradation of MB dye pollutant. Moreover, the prepared ZnO NPs demonstrated efficient antibacterial and antioxidant activities. Surface modifying reagent molecules from the extract resulted in better antibacterial activity, which may be due to the differences in the release of Zn²⁺ ions and the production of reactive oxygen species. The results of our investigation demonstrated that biosynthesized ZnO NPs possess promising potential in medical care, food packaging, and industrial applications as an alternative to chemical compounds. Further experiments should be performed, including in vivo measurements, and side effects of ingesting this compound should be thoroughly investigated.

Author Contributions: S.A. and H.-H.P. writing—original draft preparation; M.S.G., C.L., W.H. and M.J.T. writing—review and editing; H.A. and M.H.M.A. data curation. All authors have read and agreed to the published version of the manuscript.

Funding: This research was funded by Ministry of Science and ICT (2018M3D1A1058536). This work was also funded by the Korea government (MSIT) (No. 2019R1A2C2087604), and by the third Stage of Brain Korea 21 Plus Project in 2018.

Acknowledgments: This research was funded by Ministry of Science and ICT (2018M3D1A1058536). This work was also funded by the Korea government (MSIT) (No. 2019R1A2C2087604), and by the third Stage of Brain Korea 21 Plus Project in 2018.

Conflicts of Interest: The authors declare no conflict of interest.

References

1. Yusof, H.M.; Mohamad, R.; Zaidan, U.H.; Rahman, N.A.A. Abdul Rahman, Sustainable microbial cell nanofactory for zinc oxide nanoparticles production by zinc-tolerant probiotic *Lactobacillus plantarum* strain TA4. *Microb. Cell Fact.* **2020**, *19*, 1–17.
2. Podasca, V.-E.; Damaceanu, M.-D. Photopolymerized Films with ZnO and Doped ZnO Particles Used as Efficient Photocatalysts in Malachite Green Dye Decomposition. *Appl. Sci.* **2020**, *10*, 1954. [[CrossRef](#)]
3. Oh, S.; Kim, J. Correlation between the Morphology of ZnO Layers and the Electroluminescence of Quantum Dot Light-Emitting Diodes. *Appl. Sci.* **2019**, *9*, 4539. [[CrossRef](#)]
4. Lee, C.G.; Na, K.H.; Kim, W.T.; Park, D.C.; Yang, W.H.; Choi, W.Y. TiO₂/ZnO Nanofibers Prepared by Electrospinning and Their Photocatalytic Degradation of Methylene Blue Compared with TiO₂ Nanofibers. *Appl. Sci.* **2019**, *9*, 3404. [[CrossRef](#)]
5. Khan, H.; Sakharkar, M.; Nayak, A.; Kishore, U.; Khan, A. *Nanoparticles for Biomedical Applications: An Overview*; Elsevier Ltd.: Amsterdam, The Netherlands, 2018; pp. 357–377.
6. Vinardell, M.P.; Llanas, H.; Marics, L.; Mitjans, M. In Vitro Comparative Skin Irritation Induced by Nano and Non-Nano Zinc Oxide. *Nanomaterials* **2017**, *7*, 56. [[CrossRef](#)]

7. Hernández, R.; Hernández-Reséndiz, J.R.; Martínez-Chávez, A.; Velázquez-Castillo, R.; Escobar-Alarcón, L.; Esquivel, K. X-ray diffraction Rietveld structural analysis of Au–TiO₂ powders synthesized by sol–gel route coupled to microwave and sonochemistry. *J. Sol-Gel Sci. Technol.* **2020**, *93*, 1–14. [[CrossRef](#)]
8. Mazhdi, M.; Tafreshi, M. The effects of gadolinium doping on the structural, morphological, optical, and photoluminescence properties of zinc oxide nanoparticles prepared by co-precipitation method. *Appl. Phys. A* **2018**, *124*, 863. [[CrossRef](#)]
9. Kołodziejczak-Radzimska, A.; Jesionowski, T. Zinc oxide—from synthesis to application: A review. *Materials* **2014**, *7*, 2833–2881.
10. Abdolhoseinzadeh, A.; Sheibani, S. Enhanced photocatalytic performance of Cu₂O nano-photocatalyst powder modified by ball milling and ZnO. *Adv. Powder Technol.* **2020**, *31*, 40–50. [[CrossRef](#)]
11. Yusof, H.M.; Mohamad, R.; Zaidan, U.H. Microbial synthesis of zinc oxide nanoparticles and their potential application as an antimicrobial agent and a feed supplement in animal industry: A review. *J. Anim. Sci. Biotechnol.* **2019**, *10*, 57. [[CrossRef](#)] [[PubMed](#)]
12. Awwad, A.M.; Amer, M.W.; Salem, N.M.; Abdeen, A.O. Green synthesis of zinc oxide nanoparticles (ZnO-NPs) using *Ailanthus altissima* fruit extracts and antibacterial activity. *Chem. Int.* **2020**, *6*, 151–159.
13. Yuan, H.; Ma, Q.; Ye, L.; Piao, G. The traditional medicine and modern medicine from natural products. *Molecules* **2016**, *12*, 559. [[CrossRef](#)] [[PubMed](#)]
14. Sruthi, S.; Ashtami, J.; Mohanan, P. Biomedical application and hidden toxicity of Zinc oxide nanoparticles. *Mater. Today Chem.* **2018**, *10*, 175–186. [[CrossRef](#)]
15. Iravani, S. Green synthesis of metal nanoparticles using plants. *Green Chem.* **2011**, *13*, 2638–2650. [[CrossRef](#)]
16. Barabadi, H.; Tajani, B.; Moradi, M.; Kamali, K.D.; Meena, R.; Honary, S.; Mahjoub, M.A.; Saravanan, M. Penicillium Family as Emerging Nanofactory for Biosynthesis of Green Nanomaterials: A Journey into the World of Microorganisms. *J. Clust. Sci.* **2019**, *30*, 843–856. [[CrossRef](#)]
17. Ahmed, S.; Chaudhry, S.A.; Ikram, S. A review on biogenic synthesis of ZnO nanoparticles using plant extracts and microbes: A prospect towards green chemistry. *J. Photoch. Photobiol. B.* **2017**, *166*, 272–284. [[CrossRef](#)] [[PubMed](#)]
18. Garrosa, M.; Jiménez, P.; Tejero, J.; Cabrero, P.; Cordoba-Diaz, D.; Quinto, E.J.; Gayoso, M.J.; Girbés, T. Toxicity of the anti-ribosomal lectin ebulin f in lungs and intestines in elderly mice. *Toxins* **2015**, *7*, 367–379. [[CrossRef](#)]
19. Sujitha, M.V.; Kannan, S. Green synthesis of gold nanoparticles using citrus fruits (*Citrus limon*, *Citrus reticulata* and *Citrus sinensis*) aqueous extract and its characterization. *Spectrochim. Acta A Mol. Biomol. Spectrosc.* **2013**, *102*, 15–23. [[CrossRef](#)]
20. Kaviya, S.; Santhanalakshmi, J.; Viswanathan, B.; Muthumary, J.; Srinivasan, K. Biosynthesis of silver nanoparticles using *Citrus sinensis* peel extract and its antibacterial activity. *Spectrochim. Acta A Mol. Biomol. Spectrosc.* **2011**, *79*, 594–598. [[CrossRef](#)]
21. Amanulla, A.M.; Sundaram, R. Green synthesis of TiO₂ nanoparticles using orange peel extract for antibacterial, cytotoxicity and humidity sensor applications. *Mater. Today Proc.* **2019**, *8*, 323–331. [[CrossRef](#)]
22. Patil, B.N.; Taranath, T.C. *Limonia acidissima* L. leaf mediated synthesis of zinc oxide nanoparticles: A potent tool against *Mycobacterium tuberculosis*. *Int. J. Mycobacteriol.* **2016**, *5*, 197–204. [[CrossRef](#)] [[PubMed](#)]
23. Kumar, H.K.N.; Mohana, N.C.; Nuthan, B.R.; Ramesha, K.P.; Rakshith, D.R.; Geetha, N.; Satich, S. Phyto-mediated synthesis of zinc oxide nanoparticles using aqueous plant extract of *Ocimum americanum* and evaluation of its bioactivity. *SN Appl. Sci.* **2019**, *1*, 651. [[CrossRef](#)]
24. Raja, A.; AshokKumar, S.; Marthandam, R.P.; Jayachandiran, J.; Khatiwada, C.P.; Kaviyarasu, K.; Raman, R.G.; Swaminathan, M.; Kathiwada, C.P. Eco-friendly preparation of zinc oxide nanoparticles using *Tabernaemontana divaricata* and its photocatalytic and antimicrobial activity. *J. Photochem. Photobiol. B Biol.* **2018**, *181*, 53–58. [[CrossRef](#)] [[PubMed](#)]
25. Pavithra, N.; Lingaraju, K.; Raghu, G.; Nagaraju, G. *Citrus maxima* (pomelo) juice mediated eco-friendly synthesis of ZnO nanoparticles: Applications to photocatalytic, electrochemical sensor and antibacterial activities. *Spectrochim. Acta A* **2017**, *185*, 11–19. [[CrossRef](#)]
26. Steffy, K.; Shanthy, G.; Maroky, A.; Selvakumar, S. Enhanced antibacterial effects of green synthesized ZnO NPs using *Aristolochia indica* against multidrug resistant bacterial pathogens from diabetic foot ulcer. *J. Infect. Public Health.* **2018**, *11*, 463–471. [[CrossRef](#)]
27. Attar, A.; Yapaöz, M.A. Biomimetic synthesis, characterization and antibacterial efficacy of ZnO and Au nanoparticles using echinacea flower extract precursor. *Mater. Res. Express.* **2018**, *5*, 055403. [[CrossRef](#)]

28. Mohammadi-Aloucheh, R.; Habibi-Yangjeh, A.; Bayrami, A.; Latifi-Navid, S.; Asadi, A. Green synthesis of ZnO and ZnO/CuO nanocomposites in *Mentha longifolia* leaf extract: Characterization and their application as antibacterial agents. *J. Mater. Sci. Mater. Electron.* **2018**, *29*, 13596–13605. [[CrossRef](#)]
29. Karaköse, E.; Çolak, H. Structural, electrical, and antimicrobial characterization of green synthesized ZnO nanorods from aqueous *Mentha* extract. *MRS Commun.* **2018**, *8*, 577–585. [[CrossRef](#)]
30. Padalia, H.; Baluja, S.; Chanda, S. Effect of pH on size and antibacterial activity of *Salvadora oleoides* leaf extract-mediated synthesis of zinc oxide nanoparticles. *BioNanoScience* **2017**, *7*, 40–49. [[CrossRef](#)]
31. Supraja, N.; Prasad, T.N.K.V.; Krishna, T.G.; David, E. Synthesis, characterization, and evaluation of the antimicrobial efficacy of *Boswellia ovalifoliolata* stem bark-extract-mediated zinc oxide nanoparticles. *Appl. Nanosci.* **2016**, *6*, 581–590. [[CrossRef](#)]
32. Zare, E.; Pourseyedi, S.; Khatami, M.; Darezereshki, E. Simple biosynthesis of zinc oxide nanoparticles using nature's source, and its in vitro bioactivity. *J. Mol. Struct.* **2017**, *1146*, 96–103. [[CrossRef](#)]
33. Bala, N.; Saha, S.; Chakraborty, M.; Maiti, M.; Das, S.; Basu, R.; Nandy, P. Green synthesis of zinc oxide nanoparticles using *Hibiscus subdariffa* leaf extract: Effect of temperature on synthesis, anti-bacterial activity and antidiabetic activity. *RSC Adv.* **2015**, *5*, 4993–5003. [[CrossRef](#)]
34. Paul, B.; Vadivel, S.; Dhar, S.S.; Debbarma, S.; Kumaravel, M. One-pot green synthesis of zinc oxide nano rice and its application as sonocatalyst for degradation of organic dye and synthesis of 2-benzimidazole derivatives. *J. Phys. Chem. Solids* **2017**, *104*, 152–159. [[CrossRef](#)]
35. Shokrzadeh, M.; Saravi, S.S.S. The chemistry, pharmacology and clinical properties of *Sambucus ebulus*: A review. *J. Med. Plants Res.* **2010**, *4*, 95–103.
36. Alamdari, S.; Ghamsari, M.S.; Tafreshi, M.J. Optimization of Gallium concentration to improve the performance of ZnO nanopowders for nanophotonic applications. *Ceram. Int.* **2020**, *46*, 4484–4492. [[CrossRef](#)]
37. Alamdari, S.; Karkhaneh, A.; Tafreshi, M.J.; Ghamsari, M.S. Ultra-thin Hafnium doped ZnO films with enhanced optical transparency and electrical conductivity. *Mater. Res. Express* **2019**, *6*, 055020. [[CrossRef](#)]
38. Ghamsari, M.S.; Alamdari, S.; Razzaghi, D.; Pirlar, M.A. ZnO nanocrystals with narrow-band blue emission. *J. Lumin.* **2019**, *205*, 508–518. [[CrossRef](#)]
39. Alamdari, S.; Tafreshi, M.; Ghamsari, M.S. Strong yellow-orange emission from aluminum and Indium co-doped ZnO nanostructures with potential for increasing the color gamut of displays. *Appl. Phys. A.* **2019**, *125*, 165. [[CrossRef](#)]
40. Alamdari, S.; Tafreshi, M.J.; Ghamsari, M.S. The effects of indium precursors on the structural, optical and electrical properties of nanostructured thin ZnO films. *Mater. Lett.* **2017**, *197*, 94–97. [[CrossRef](#)]
41. Ghamsari, M.S.; Alamdari, S.; Han, W.; Park, H.-H. Park, Impact of nanostructured thin ZnO film in ultraviolet protection. *Int. J. Nanomed.* **2017**, *12*, 207–216. [[CrossRef](#)]
42. Alamdari, S.; Ghamsari, M.S.; Ara, M.M.; Efafi, B. Highly concentrated IZO colloidal nanocrystals with blue/orange/red three-color emission. *Mater. Lett.* **2015**, *158*, 202–204. [[CrossRef](#)]
43. Alamdari, S.; Sasani Ghamsari, M.; Jafar Tafreshi, M. Synthesis, characterization and gas sensing properties of In-doped ZnO nanopowders. *Nanochem. Res.* **2017**, *2*, 198–204.
44. Vafaei, M.; Ghamsari, M.S.; Radiman, S. Highly concentrated zinc oxide nanocrystals sol with strong blue emission. *J. Lumin.* **2011**, *131*, 155–158. [[CrossRef](#)]
45. Bauer, A.W.; Kirby, W.M.M.; Sherris, J.C.; Turck, M. Antibiotic susceptibility testing by a standardized single disk method. *Am. J. Clin. Pathol.* **1966**, *45*, 493–496. [[CrossRef](#)]
46. Pick, E.; Mizel, D. Rapid microassays for the measurement of superoxide and hydrogen peroxide production by macrophages in culture using an automatic enzyme immunoassay reader. *J. Immunol. Methods* **1981**, *46*, 211–226. [[CrossRef](#)]
47. Cope, J.O.; Campbell, I.D. Electron spin resonance observations of oxygen chemisorption on zinc oxide. *J. Chem. Soc. Faraday Trans.* **1973**, *1*, 1–9. [[CrossRef](#)]
48. Kaftelen, H.; Ocakoglu, K.; Thomann, R.; Tu, S.; Weber, S.; Erdem, E. EPR and photoluminescence spectroscopy studies on the defect structure of ZnO nanocrystals. *Phys. Rev. B* **2012**, *86*, 014113. [[CrossRef](#)]
49. Efafi, B.; Ghamsari, M.S.; Aberoumand, M.A.; Ara, M.M.; Ghamsari, A.H.S.; Rad, H.H. Aluminum doped ZnO sol-gel derived nanocrystals: Raman spectroscopy and solid solubility characterization. *Phys. Status Solidi A* **2014**, *211*, 2426–2430. [[CrossRef](#)]

50. Sundrarajan, M.; Ambika, S.; Bharathi, K. Plant-extract mediated synthesis of ZnO nanoparticles using *Pongamia pinnata* and their activity against pathogenic bacteria. *Adv. Powder Technol.* **2015**, *26*, 1294–1299. [[CrossRef](#)]
51. Senthilkumar, N.; Nandhakumar, E.; Priya, P.; Soni, D.; Vimalan, M.; Potheher, I.V. Synthesis of ZnO nanoparticles using leaf extract of *Tectona grandis* (L.) and their anti-bacterial, anti-arthritis, anti-oxidant and in vitro cytotoxicity activities. *New J. Chem.* **2017**, *41*, 10347–10356. [[CrossRef](#)]
52. Stan, M.; Popa, A.; Toloman, D.; Silipas, T.-D.; Vodnar, D.C. Antibacterial and antioxidant activities of ZnO nanoparticles synthesized using extracts of *Allium sativum*, *Rosmarinus officinalis* and *Ocimum basilicum*. *Acta Met. Sin. Engl. Lett.* **2016**, *29*, 228–236. [[CrossRef](#)]
53. Romero, R.; López-Ibáñez, R.; Dalchiele, E.A.; Ramos-Barrado, J.R.; Martín, F.; Leinen, D. Compositional and physico-optical characterization of 0–5%Al-doped zinc oxide films prepared by chemical spray pyrolysis. *J. Phys. D Appl. Phys.* **2010**, *43*, 095303. [[CrossRef](#)]
54. Al-Gaashani, R.; Radiman, S.; Daud, A.; Tabet, N.; Al-Douri, Y. XPS and optical studies of different morphologies of ZnO nanostructures prepared by microwave methods. *Ceram. Int.* **2013**, *39*, 2283–2292. [[CrossRef](#)]
55. Dayioglu, H.; Kut, D.; Merdan, N.; Eyupoglu, S. The effect of dyeing properties of fixing agent and plasma treatment on silk fabric dyed with natural dye extract obtained from *Sambucus ebulus* L. plant. *Procedia Soc. Behav. Sci.* **2015**, *195*, 1609–1617. [[CrossRef](#)]
56. Vafaei, M.; Ghamsari, M.S. Preparation and characterization of ZnO nanoparticles by a novel sol–gel route. *Mater. Lett.* **2007**, *61*, 3265–3268. [[CrossRef](#)]
57. Wetchakun, N.; Chaiwichain, S.; Inceesungvorn, B.; Pingmuang, K.; Phanichphant, S.; Minett, A.I.; Chen, J. BiVO₄/CeO₂ nanocomposites with high visible-light-induced photocatalytic activity. *ACS Appl. Mater. Interfaces* **2012**, *4*, 3718–3723. [[CrossRef](#)]
58. Liang, H.; Tai, X.; Du, Z.; Yin, Y. Enhanced photocatalytic activity of ZnO sensitized by carbon quantum dots and application in phenol wastewater. *Opt. Mater.* **2020**, *100*, 109674. [[CrossRef](#)]
59. Ngoepe, N.; Mbita, Z.; Mathipa, M.; Mketi, N.; Ntsendwana, B.; Hintsho-Mbita, N. Biogenic synthesis of ZnO nanoparticles using *Monsonia burkeana* for use in photocatalytic, antibacterial and anticancer applications. *Ceram. Int.* **2018**, *44*, 16999–17000. [[CrossRef](#)]
60. Meena, S.; Vaya, D.; Das, B.K. Photocatalytic degradation of Malachite Green dye by modified ZnO nanomaterial. *Bull. Mater. Sci.* **2016**, *39*, 1735–1743. [[CrossRef](#)]
61. Nava, O.; Morales, P.L.; Gutiérrez, C.M.G.; Vilchis-Nestor, A.; Castro-Beltrán, A.; Mota-González, M.; Olivas, A. Influence of *Camellia sinensis* extract on zinc oxide nanoparticle green synthesis. *J. Mol. Struct.* **2017**, *1134*, 121–125. [[CrossRef](#)]
62. Ambika, S.; Sundrarajan, M. Antibacterial behaviour of *Vitex negundo* extract assisted ZnO nanoparticles against pathogenic bacteria. *J. Photochem. Photobiol. B Biol.* **2015**, *146*, 52–57. [[CrossRef](#)] [[PubMed](#)]
63. Sinha, R.; Karan, R.; Sinha, A.; Khare, S.K. Interaction and nanotoxic effect of ZnO and Ag nanoparticles on mesophilic and halophilic bacterial cells. *Bioresour. Technol.* **2011**, *102*, 1516–1520. [[CrossRef](#)] [[PubMed](#)]
64. Jones, N.; Ray, B.; Ranjit, K.T.; Manna, A.C. Antibacterial activity of ZnO nanoparticle suspensions on a broad spectrum of microorganisms. *FEMS Microbiol. Lett.* **2008**, *297*, 71–76. [[CrossRef](#)] [[PubMed](#)]
65. Jayaseelan, C.; Rahuman, A.A.; Kirthi, A.V.; Marimuthu, S.; Santhoshkumar, T.; Bagavan, A.; Gaurav, K.; Karthik, L.; Rao, K.V.B. Novel microbial route to synthesize ZnO nanoparticles using *Aeromonas hydrophila* and their activity against pathogenic bacteria and fungi. *Spectrochim. Acta A* **2012**, *90*, 78–84. [[CrossRef](#)]
66. Singh, V.; Mishra, A.K. White light emission from vegetable extracts. *Sci. Rep.* **2015**, *5*, 11118. [[CrossRef](#)]
67. Padmavath, N.; Vijayaraghavan, R. Enhanced bioactivity of ZnO nanoparticles—an antimicrobial study. *Sci. Technol. Adv. Mater.* **2008**, *9*, 035004. [[CrossRef](#)]
68. Fernández, L.; Hancock, R.E.W. Adaptive and mutational resistance: Role of porins and efflux pumps in drug resistance. *Clin. Microbiol. Rev.* **2012**, *25*, 661. [[CrossRef](#)]
69. Yamamoto, O.; Komatsu, M.; Sawai, J.; Nakagawa, Z. Antibacterial activity of ZnO particle with crystallographic orientation. *J. Mater. Sci. Mater. Med.* **2008**, *19*, 1407–1412.
70. Luo, F.; Yang, D.; Chen, Z.; Megharaj, M.; Naidu, R. One-step green synthesis of bimetallic Fe/Pd nanoparticles used to degrade Orange II. *J. Hazard. Mater.* **2016**, *3030*, 145–153. [[CrossRef](#)]
71. Mittal, A.K.; Chisti, Y.; Banerjee, U.C. Synthesis of metallic nanoparticles using plant extracts. *Biotechnol. Adv.* **2013**, *31*, 346–356. [[CrossRef](#)]

72. Weng, X.; Guo, M.; Luo, F.; Chen, Z. One-step green synthesis of bimetallic Fe/Ni nanoparticles by eucalyptus leaf extract: Biomolecules identification, characterization and catalytic activity. *Chem. Eng. J.* **2017**, *308*, 904–911. [[CrossRef](#)]
73. Wu, J.M.; Kao, W.T. Heterojunction nanowires of $Ag_xZn_{1-x}O$ -ZnO photocatalytic and antibacterial activities under visible-light and dark conditions. *J. Phys. Chem. C.* **2015**, *119*, 1433–1441. [[CrossRef](#)]
74. Umar, H.; Kavaz, D.; Rizaner, N. Biosynthesis of zinc oxide nanoparticles using *Albizia lebbeck* stem bark, and evaluation of its antimicrobial, antioxidant, and cytotoxic activities on human breast cancer cell lines. *Int. J. Nanomed.* **2019**, *14*, 87–100. [[CrossRef](#)] [[PubMed](#)]
75. Kumar, N.H.; Murali, M.; Satish, A.; Singh, S.B.; Gowtham, H.G.; Mahesh, H.M.; Lakshmeesha, T.R.; Amruthesh, K.N.; Jagannath, S. Bioactive and Biocompatible Nature of Green Synthesized Zinc Oxide Nanoparticles from *Simarouba glauca* DC.: An Endemic Plant to Western Ghats, India. *J. Clust. Sci.* **2020**, *31*, 523–534. [[CrossRef](#)]
76. Arvanag, F.M.; Bayrami, A.; Habibi-Yangjeh, A.; Pouran, S.R.; Mohammadi, F. Pouran, A comprehensive study on antidiabetic and antibacterial activities of ZnO nanoparticles biosynthesized using *Silybum marianum* L. seed extract. *Mater. Sci. Eng. C* **2019**, *97*, 397–405. [[CrossRef](#)]
77. Parashant, G.K.; Prashant, P.A.; Utpal, B.; Manoj, G.; Nagabhushana, B.M.; Ananda, S.; Krishnaiah, G.M.; Sathyananda, H.M. In vitro antibacterial and cytotoxicity studies of ZnO nanoparticles prepared by combustion assisted facile green synthesis. *Karbala Int. J. Mod. Sci.* **2015**, *1*, 67–77.
78. Rogers, N.J.; Apte, S.C.; Batley, G.E.; Gadd, G.E.; Casey, P.S. Comparative toxicity of nanoparticulate ZnO, bulk ZnO, and ZnCl₂ to a freshwater microalga subcapitata: The importance of particle solubility. *Environ. Sci. Technol.* **2007**, *41*, 8484–8490.
79. Agarwal, H.; Menon, S.; Kumar, S.V.; Rajeshkumar, S. Mechanistic study on antibacterial action of zinc oxide nanoparticles synthesized using green route. *Chemico-Biol. Interact.* **2018**, *286*, 60–70. [[CrossRef](#)]
80. Arakha, M.; Saleem, M.; Mallick, B.C.; Jha, S. The effects of interfacial potential on antimicrobial propensity of ZnO nanoparticle. *Sci. Rep.* **2015**, *5*, 9578. [[CrossRef](#)]
81. Leung, Y.H.; Chan, C.M.N.; Ng, A.M.C.; Chan, H.T.; Chiang, M.W.L. Antibacterial activity of ZnO nanoparticles with a modified surface under ambient illumination. *Nanotechnology* **2012**, *23*, 475703. [[CrossRef](#)]
82. Peng, X.; Palma, S.; Fisher, N.S.; Wong, S.S. Effect of morphology of ZnO nanostructures on their toxicity to marine algae. *Aquat. Toxicol.* **2011**, *102*, 186–196. [[CrossRef](#)] [[PubMed](#)]
83. Sangeetha, G.; Rajeswari, S.; Venkatesh, R. Green synthesized ZnO nanoparticles against bacterial and fungal pathogens. *Prog. Nat. Sci. Mater. Int.* **2012**, *22*, 693–700.
84. Susheela, S.; Sunil, K.; Bulchandini, B.D.; Shalini, T.; Shelza, B. Green synthesized ZnO nanoparticles against bacterial and fungal pathogens. *Int. J. Biotechnol. Bioeng. Res.* **2013**, *4*, 341–346.

